Traveling wave dielectrophoresis micropump based on the dispersion of a capacitive electrode layer

M. Marczak, H. Diesinger

Traveling wave dielectrophoresis micropump based on the dispersion of a capacitive electrode layer

Cite as: J. Appl. Phys. **105**, 124511 (2009); https://doi.org/10.1063/1.3152787
Submitted: 07 November 2008 • Accepted: 17 May 2009 • Published Online: 23 June 2009

Marcin Marczak and Heinrich Diesinger

Traveling wave dielectrophoresis micropump based on the dispersion of a capacitive electrode layer

Marcin Marczak[1,2,a)] and Heinrich Diesinger[2]
[1]*Faculty of Physics, Warsaw University of Technology, Koszykowa 75, PL-00-662 Warsaw, Poland*
[2]*Institut d'Electronique, de Microélectronique et de Nanotechnologie, CNRS UMR 8520, Dpt. ISEN, Avenue Poincaré, F-59652 Villeneuve d'Ascq, France*

(Received 7 November 2008; accepted 17 May 2009; published online 23 June 2009)

A traveling wave dielectrophoresis microfluid pump based on structural dispersion is demonstrated. The phase shift between medium polarization and applied propagating field, necessary to generate asynchronous propagative forces in dielectrophoresis, is generated by an *RC* circuit consisting of the electrode insulator and the liquid conductivity. Since the device characteristics involve only bulk properties, the micropump does not require conductivity gradient or double layers, unlike existing micropumps using electro-osmosis and electrohydrodynamic shear forces. Its frequency of maximum pumping force can be made considerably lower than the dielectric relaxation frequency of the liquid. By decomposing the traveling wave electrode array into a rudimentary *RC* model, coincidence is found between optimized pumping conditions and crossover of the impedance measured between electrode combs. By using impedance spectroscopy alternately with pumping, the frequency of the applied signal can be matched in real-time to the complex dielectric constant of the liquid to keep the pumping force maximized. © *2009 American Institute of Physics*. [DOI: 10.1063/1.3152787]

I. INTRODUCTION

The success of Lab-on-chip technology[1] depends on further miniaturization,[2] dense integration and increased cost efficiency of devices that manipulate an analyze liquid matter.[3,4] Key issues are pumping,[5,6] dosing,[7] or sorting[8,9] of different substances. Liquid pumping without moving parts by traveling electric field dates back to the 1990s when Hagedorn[10,11] demonstrated an electrohydrodynamic (EHD) micropump. The two mechanisms most often involved in lab-on-chips systems are EHD and traveling wave electro-osmotic (TWEO) pumping. EHD setups are based on electric shear forces,[12,13] requiring a conductivity gradient of the liquid and frequencies near the dielectric relaxation frequency of the (slightly) conductive liquid to introduce the phase shift between the medium polarization and the applied field necessary to exert a force. At steady state, an equilibrium is established between viscous and electrostatic shear forces, leading to the typical velocity profile with a maximum between the electrode array and cover plate. TWEO[14,15] depends on the formation of a double layer above the electrode array, leading to drag forces onto the ions at the interface in the propagating field.

The approach of this work is the application of the dielectrophoresis (DEP) particle handling technique in a propagating field[16] to a liquid volume. Instead of applying a force to a particle with a dielectric constant different from its surroundings, traveling wave DEP should inversely be able to apply a force to a liquid with a complex dielectric constant different from the surroundings by attributing the former role of the particle to the liquid volume. Although in the case of a re-entrant channel, the usual formalism consisting in treating the object as ellipsoidal body and obtaining its polarization by the Clausius–Mosotti equation as described for example by Hughes[16] cannot be applied here, it follows from exchanging the roles of particle and liquid volume that it should be possible to apply dielectrophoretic forces to pump liquid in a channel without relying on one of the previously mentioned mechanisms.

In this work, we demonstrate a microfluid pumping device consisting of interdigitated electrode combs buried below an insulating layer to generate a traveling field in a microchannel. This device distinguishes itself by operating mode that exerts a force on the channel volume independently of a conduction gradient,[13] inherent media dispersion, and double layer effects,[12,17] and its interpretation by decomposing it into an *RC* model.

The operating range in terms of relation between the operating frequency below 1 MHz and the microscopic dimensions of the device corresponds to the quasielectrostatic limit, meaning that the channel does not propagate electromagnetic waves as a hollow microwave guide does. The device produces the necessary phase lag between the applied field and the polarization of the liquid by structural dispersion due to the dielectric electrode coating and the conductivity of the ionic liquid. Inherent media dispersion is not involved, allowing the operating frequency to be chosen far below the dielectric relaxation frequency of the liquid and consequently to handle liquids of higher conductivity than the EHD approach.

For analytic modelization, the traveling wave electrode array is decomposed into a rudimentary *RC* model, with the resistance corresponding to the liquid conductivity and the capacitance to the dielectric electrode coating. Analytical treatment not only allows estimating the relation between the

a)Electronic addresses: marcin.marczak@isen.iemn.univ-lille1.fr.

dielectric properties and the frequency of the applied four phase signal to maximize pumping force, but also shows that this condition coincides with the observation of crossover of the impedance measured between electrode combs. This is confirmed experimentally. On one hand, the analytic approach fills a gap between precise numerical simulation[18–23] and the trial and error methods frequently observed in experimental implementations. On the other hand, it is demonstrated that the use of impedance spectroscopy for monitoring the matching of the frequency and liquid conductance can trigger a whole new generation of devices. If used alternately with pumping, the impedance feedback not only allows correcting tolerances in device fabrication and liquid preparation, but can also be used for compensating time dependent fluctuations in real-time, assuring continuous optimized pumping power. Previous works[17,24–26] have used impedance spectroscopy in combination with DEP only to measure the impedance of cells trapped in the channel of a DEP device, but not as a means of maximizing the dielectrophoretic pumping force.

II. DEP MODELIZATION

A. Principle of DEP pumping: Out of phase media polarization

In particle handling by DEP, an inhomogeneous field causes a polarization of a particle and at the same time of the surrounding medium.[27–29] Since the permittivities and conductivities of both materials are different, the polarization will differ, resulting in an Archimedes-like force acting on the body in the water. The particle is pushed to or repelled from the field maxima. The idea of traveling wave DEP (TWDEP) originates from linearized electrorotation[10] and consists in replacing the static field gradient by the dynamic one associated with a propagating sinusoidal field. In asynchronous TWDEP, the particle speed can be neglected with respect to the motion of the traveling wave, and the particle polarization is partly out of phase with the electric field of the traveling wave, resulting in a continuous net mean force in the propagation direction.

Following the approach of inversed roles, the objective is the pumping of liquid by polarizing it with a phase difference relative to an applied traveling field to exert a net force on the liquid. This is possible if the liquid has a complex dielectric response. In the frequency range that can easily be applied to a microarray and that we intend to work with, $f \leq 1$ MHz, ionic liquids are well described by a bulk dielectric constant consisting of a static term ϵ' and a conductivity σ

$$\epsilon_{\mathrm{liq}} = \epsilon' + i\epsilon'' = \epsilon' + \frac{i\sigma}{\omega}. \tag{1}$$

If the liquid (or other conductive material described by this model) is exposed to an electric field E_{appl}, the field inside the liquid volume is determined by the Fresnel law (equal dielectric displacement on both sides of the interface)

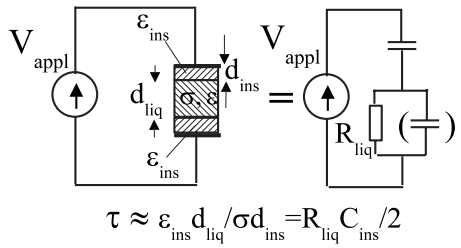

FIG. 1. Replacement circuit of a conductive material (e.g., ionic liquid) between conductive plates covered by an insulator.

$$E_{\mathrm{liq}} = E_{\mathrm{appl}}\frac{\epsilon_{\mathrm{ext}}}{\epsilon_{\mathrm{liq}}} = E_{\mathrm{appl}}\frac{\epsilon_{\mathrm{ext}}}{\epsilon' + i\frac{\sigma}{\omega}} = E_{\mathrm{appl}}\frac{\frac{\epsilon_{\mathrm{ext}}}{\epsilon'}}{1 + i\frac{1}{\omega\tau_a}}. \tag{2}$$

This shows that the polarization of the liquid is subject to decay with a time constant τ_a. The buildup of an accumulation layer at the interface screens the polarization inside the material, but the establishing of the accumulation layer is governed by the dielectric relaxation time constant $\tau_a = \epsilon'/\sigma$. The relaxation effect can give rise to a polarization with a phase shift relative to the applied field. The same time constant would be obtained as $\tau_a = R_{\mathrm{liq}}C_{\mathrm{liq}}$ if the liquid volume was considered as a RC parallel circuit consisting of the resistance and capacitance R_{liq} and C_{liq}, respectively. This can be written as functions of the physical dimensions d_{liq} of the liquid volume and its surface A if calculated in the plane geometry, and its static dielectric constant ϵ', and its conductivity σ

$$R_{\mathrm{liq}} \approx \frac{d_{\mathrm{liq}}}{A\sigma}, \tag{3}$$

$$C_{\mathrm{liq}} = \frac{A\epsilon'}{d_{\mathrm{liq}}}. \tag{4}$$

This RC element has a crossover frequency typically of 200 kHz, too high to apply with conventional cabling.

Figure 1 shows a setup where the electrodes are insulated from the liquid by a thin dielectric layer, along with the corresponding RC model. If the insulating layer is thin with respect to the liquid volume, its capacitance can be made higher than the one of the liquid, justifying neglecting the capacitance due to the static C_{liq} with respect to C_{ins}. With this approach, the equivalent electric circuit using plane capacitors and resistances leads to

$$V_{\mathrm{liq}} = V_{\mathrm{appl}}\frac{1}{1 + \frac{1}{i\omega R_{\mathrm{liq}}C_{\mathrm{ins}}/2}}, \tag{5}$$

where

$$C_{\mathrm{ins}} = \frac{A\epsilon_0\epsilon_{\mathrm{ins}}}{d_{\mathrm{ins}}}. \tag{6}$$

The voltage drop in the liquid volume is subject to a decay time constant, comparable to the field in the liquid volume exposed to a given homogeneous electric field. However, the decay time constant τ_c of this configuration is determined by the liquid resistance and the capacitance of the *insulator*

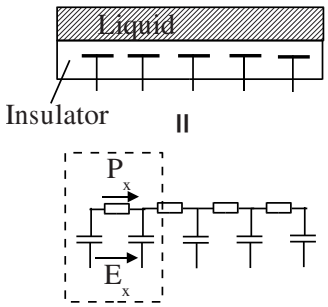

FIG. 2. Decomposition of the electrode array into an *RC* model: the isolated array covered by the ionic liquid is represented by an equivalent *RC* network. A single cell is surrounded by a box.

$$\tau_c = \frac{R_{\text{liq}} C_{\text{ins}}}{2}. \tag{7}$$

This shows that for setup with electrodes covered by a thin insulator, the time constant is higher by a factor $C_{\text{ins}}/2C_{\text{liq}}$ than for the case of the liquid exposed to an electric field. This means that in a configuration where an ionic liquid is polarized between conductive plates covered by a thin insulating layer, an out-of-phase polarization can be obtained at much lower frequency than the Maxwell–Wagner relaxation frequency for a given liquid conductivity. It will be confirmed in the following section that the operating frequency $f_{\text{crossover}} \approx 500$ kHz is far below the typical Maxwell–Wagner (200 kHz range) relaxation frequency, but still far above the double layer dispersion range ($\approx$kHz) meaning that both effects can be neglected.

B. Decomposition of the electrode array into an *RC* network

To generate a traveling wave, an array of interdigitated electrode combs is supplied with a four phase voltage. For simplicity, only the longitudinal component of electric field and media polarization in the direction of propagation are taken into account here. The equivalence between the microelectrode array and an *RC* network is shown in Fig. 2. The polarization of the ionic solution is represented by the voltage drop across the resistor and the electric longitudinal field in one cell is proportional to the voltage applied between two neighboring electrodes.

By taking into account only longitudinal components, the force onto the volume of a single cell is

$$F_x = P_x \frac{d}{dx} E_x. \tag{8}$$

The voltage, electric fields, field gradient, medium polarization, and dielectrophoretic force of the four phase signal powered microarray is indicated in Fig. 3. Curve (a) shows the applied voltage. The longitudinal electric field far above the electrode array E_{appl} can be approached as a sinusoidal wave [Fig. 3(c)]

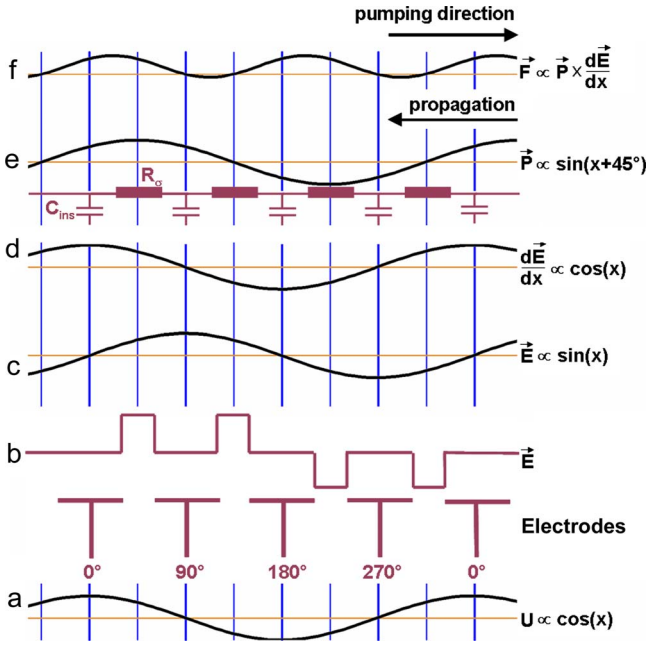

FIG. 3. (Color online) Phase relations between the applied voltage (a), the electric field [(b) and (c)], the field gradient (d), the liquid polarization (e), and the resulting force (f) acting on the liquid at $t=0$. The resulting polarization of the liquid is leading the E_x field (by the 45°) at the frequency where the pumping force is maximized. The pumping force is proportional to the mean value of the product of the polarization and the field gradient. Electric field at the electrodes level is discrete (b), which at higher distance above the electrodes will approach sinusoidal shape.

$$E_x = \frac{V_0}{L} \text{Re}\left\{ \exp i\left(k_x + \omega t - \frac{\pi}{4} \right) \right\}, \tag{9}$$

where V_0 is the peak voltage, L is the pitch, and the $\pi/4$ phase shift is due to the fact that the field maximum of the sine wave approach is just above the 90º electrode at $t=0$. In the plane of the electrodes, the field has square x dependence rather than sinusoidal [Fig. 3(b)], but at a height on the order of the pitch above the electrodes, the higher spatial frequencies are evanescent and a sine wave is approached[14] [Fig. 3(c)]. Curve (d) shows the field gradient.

The gradient is given by Eq. (10)

$$\frac{d}{dx} E_x = \frac{V_0}{L} \text{Re}\left\{ ik \exp i\left(k_x x + \omega t - \frac{\pi}{2} \right) \right\}, \tag{10}$$

and the polarization [Fig. 3(e)] of the volume element above the array along the propagation direction is

$$P_x = \frac{V_0}{L_R} \text{Re}\left\{ \frac{R_{\text{liq}}}{R_{\text{liq}} + \frac{1}{i\omega C_{\text{ins}}}} \exp i\left(k_x x + \omega t - \frac{\pi}{4} \right) \right\}, \tag{11}$$

where L_R is an effective cell length to take into account nonplanar geometry. In order to obtain a net force, meaning a nonvanishing mean value of Eq. (8), if integrated over a time period $T = 2\pi/\omega$, the imaginary part of the *RC* voltage divider

$$\text{Im}\left\{ \frac{R_{\text{liq}}}{R_{\text{liq}} + \frac{1}{i\omega C_{\text{ins}}}} \right\}, \tag{12}$$

must be maximized, meaning

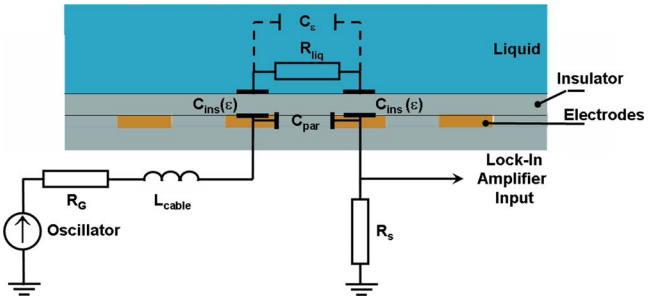

FIG. 4. (Color online) The cell with liquid inside can be represented as a RC circuit. The liquid is represented by R_{liq} and the insulator by C_{ins}. Between the electrodes appears the parasitic capacitance C_{par}. R_s is a shunt resistance, which is a part of a voltage divider used in our equations. R_G is the impedance of the generator. L_{cable} is the inductance of the wiring.

$$R_{\mathrm{liq}} = \frac{1}{\omega C_{\mathrm{ins}}}, \tag{13}$$

which is the case at the crossover frequency of the overall cell impedance $Z = R_{\mathrm{liq}} + 1/i\omega C_{\mathrm{ins}}$.

Including Eqs. (3) and (6) the condition given by Eq. (13) then becomes

$$\sigma = \omega \epsilon_0 \epsilon_{\mathrm{ins}} \frac{L_R}{d}. \tag{14}$$

As can be expected from the phase shift between the medium polarization and applied field, the pumping direction will be opposite to the traveling direction of the field.

III. EXPERIMENT

A. Experimental measurement of the crossover frequency

To experimentally measure the cell impedance and to find its crossover frequency, the setup needs to be modeled by taking into account other reactive components in proximity of the cell and in the cabling, as indicated in Fig. 4. Between the electrodes appears a parasitic capacitance, which has to be taken into account by the model in order to resolve for the RC of interest, i.e., R_{liq}, C_{ins}, and C_{par}. R_s is a shunt resistance, which is a part of a voltage divider used in our equations. R_G is the internal impedance of the generator. L is the inductance of the wiring. The shunt voltage U_S as function of the applied oscillator voltage U_{OSC} is given by the voltage divider equation

$$U_s = \frac{R_S}{R_S + i\omega L + \underbrace{\left(R_{liq} + \frac{1}{i\omega C_{\mathrm{ins}}}\right) \| \frac{1}{i\omega C_{\mathrm{par}}}}_{Z_{\mathrm{cell}}}} U_{\mathrm{osc}}. \tag{15}$$

To obtain L we have removed the cell from the setup and shortcut the connecting wires ($Z_{\mathrm{cell}}=0$). We resolve Eq. (15) for ωL

$$\omega L = -\frac{\mathrm{Im}[U_S] U_{\mathrm{OSC}} R_S}{U_S^2}. \tag{16}$$

$L = 2\ \mu\mathrm{H}$ is obtained from the slope after plotting Eq. (16) over ω.

Knowing the values of L Eq. (15) can be resolved for the real and imaginary part of the cell impedance Z_{cell}

$$\mathrm{Re}[Z] = \frac{\mathrm{Re}[U_S] U_{\mathrm{OSC}} R_S}{U_S^2} - R_G - R_S, \tag{17}$$

$$\mathrm{Im}[Z] = -\frac{\mathrm{Re}[U_S] U_{\mathrm{OSC}} R_S}{U_S^2} - \omega L. \tag{18}$$

Next, the cell without liquid ($R_{\mathrm{liq}}=\infty$) is connected and the measurement is repeated. This time Eq. (15) is resolved for ωC_{par}

$$\omega C_{\mathrm{par}} = \left(\frac{\mathrm{Im}[U_S] U_{\mathrm{OSC}} R_S}{U_S^2} + \omega L\right)^{-1}. \tag{19}$$

where $C_{\mathrm{par}} = 31$ pF is obtained from the slope after plotting the expression (19) over ω.

To compensate for the effect of C_{par} in order to obtain the characteristics of R_{liq} and C_{ins}, it is necessary to switch the cell impedance to admittance.

$$Y_{C_{\mathrm{par}}} = i\omega C, \tag{20}$$

$$|Z| = [(\mathrm{Re}[Z])^2 + (\mathrm{Im}[Z])^2]^{1/2},$$

$$\Theta_Z = \arctan\frac{\mathrm{Im}[Z]}{\mathrm{Re}[Z]}, \tag{21}$$

$$\mathrm{Re}[Y] = \frac{\cos(-\Theta_Z)}{|Z|},$$

$$\mathrm{Im}[Y] = \frac{\sin(-\Theta_Z)}{|Z|}. \tag{22}$$

Now the admittance of R_{liq} in series with C_{ins} is obtained

$$\mathrm{Re}[Y_{\mathrm{Corr}}] = \mathrm{Re}[Y],$$

$$\mathrm{Im}[Y_{\mathrm{Corr}}] = \mathrm{Im}[Y] - \mathrm{Im}[Y_{C_{\mathrm{par}}}]. \tag{23}$$

Plotting $\mathrm{Im}[Y_{\mathrm{Corr}}]$ versus $\mathrm{Re}[Y_{\mathrm{Corr}}]$ will result in a Nyquist plot corresponding to the RC circuit consisting of R_{liq} and C_{ins} (see Sec. IV).

B. Chip preparation

In the experimental implementation the electrode array shown in Fig. 5 was used. A 200 nm high DEP electrode array (layer 1) was buried in SiO_2 (500 nm) deposited on a ⟨100⟩ n-type silicon wafer. The array was covered with 150 nm of Si_3N_4 and interconnection holes (layer 2) were etched with CHF_3/CF_4. Next, the bus lines (layer 3) of 150 nm height were deposited, simultaneously being connected to the electrodes via interconnections. Another layer of 200 nm of Si_3N_4 (layer 4) was deposited and area over contact pads was etched with CHF_3/CF_4 to uncover the electrodes pads necessary to connect the four phase supply voltage. Finally the 60 μm high microchannels were made using SU8 resist

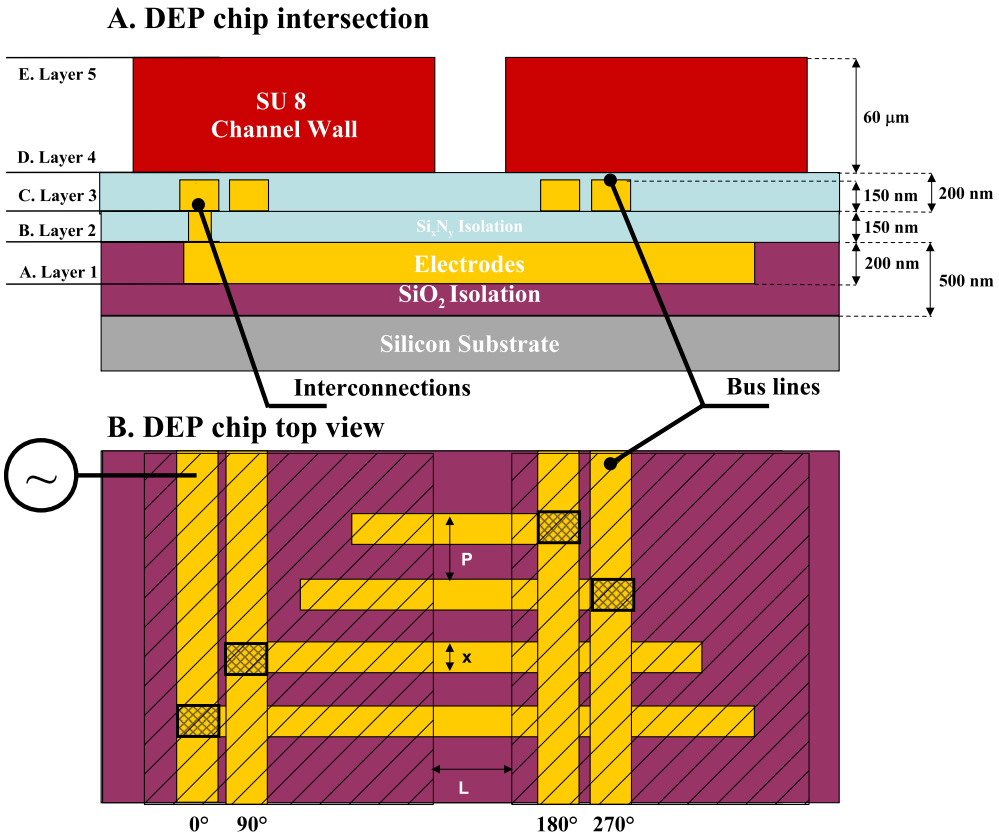

FIG. 5. (Color online) Dielectrophoresis chip intersection (a) and top view (b). Five photolithography levels are shown.

(layer 5). The width of the channel (L) varied from 8 to 30 μm and electrode sizes (x) (same as their spacing) from 2 to 10 μm. The four phase interdigitated electrode design of Fig. 5 was repeated 25 times (periodicity $P=2x$).

C. Liquid preparation

2 ml of de-ionized water and 0.5 μl of NaCl 0.9% solution (Gilbert, France) was added. Resulting liquid conductivity was estimated at $\sigma=0.001(S/m)$. After the impedance spectroscopy measurements (see the next chapter), 0.1 ml suspension of latex beads of 10 μm in diameter (Fluoresbrite™) was added to visualize the motion of the liquid.

D. DEP/impedance spectroscopy setup

A DEP chip has been connected to a electrical switch [Fig. 6 DEP/impedance spectroscopy (IS) switch]. This switch is responsible for change between traveling DEP (Fig. 6 bottom) and impedance spectroscopy mode (Fig. 6 top). For the first mode the signal is generated by a HP8904a multifunction generator. Since it is only able to generate two signals, a 180° inverter had to be designed. Two ac signals with phases 0° and 90° are generated by the multifunction generator and connected to the input of the inverter, providing four signals with the same amplitude but different phases 0°, 90°, 180°, and 270°. These signals are applied to the electrodes in the DEP chip to generate a traveling field. For the impedance measurement, the signal is generated by a 7280 DSP lock-in amplifier. It is connected only to two neighboring electrode combs. Furthermore, we added the possibility to switch between all possible combinations of the electrode comb pairs in impedance spectroscopy mode (not shown for simplicity). This has been necessary to detect symmetry problems and short-circuits between the electrodes. A spectrum is acquired in the 0–2 MHz range (for $V_{OSC}=0.02$ V), reading the voltage drop on the shunt resistance R_s. By performing the current spectroscopy between two electrode combs rather than on the unit cell as indicated in Fig. 4, the reasoning of Sec. III A remains valid. By applying the necessary corrections, the impedance crossover frequency, at witch the liquid pumping is predicted to be optimized (see Sec. III A), is obtained. The determined frequency is then entered into the function generator and the mode is set to traveling field DEP, using a sinusoidal drive voltage $V_{pp}=8$ V. With these working parameters, the DEP chip is placed under optical microscope. A magnification of 200× allows us to observe the motion of the suspension of the latex beads described in Sec. III C.

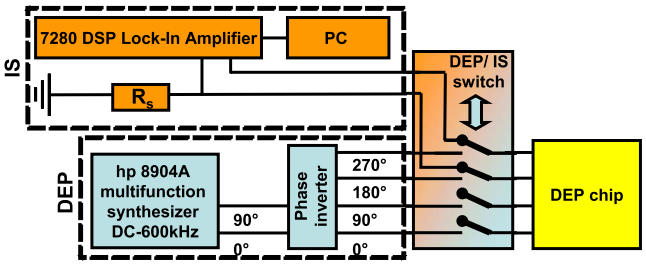

FIG. 6. (Color online) Block diagram of a traveling DEP setup (TWDEP) allowing to commute the electrode array between impedance spectroscopy measurement (IS) or four phase power supply (DEP).

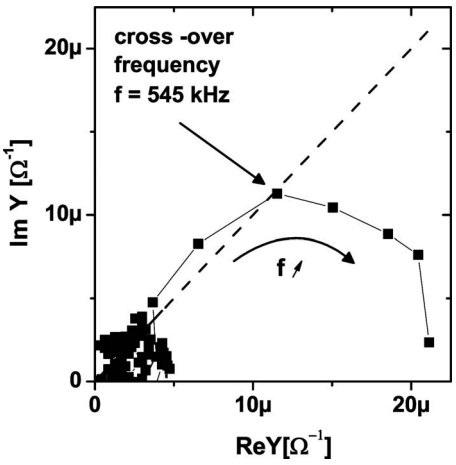

FIG. 7. Nyquist plot. The crossover frequency is found to be at $f = 545$ kHz.

IV. RESULTS

A. Nyquist plot of C_{ins} and R_{liq} serial circuit

Plotting the $\mathrm{Im}[Y_{\mathrm{Corr}}]$ versus $\mathrm{Re}[Y_{\mathrm{Corr}}]$ will give a Nyquist plot (Fig. 7). The intersection of the Nyquist plot with the unity slope line yields a crossover frequency of $f = 545$ kHz.

B. Movie sequence

Figure 8 shows screens-shots of the movie presenting the liquid being pumped with an applied frequency $f = 545$ kHz. It visualizes a bead that is dragged with the liquid. To proof the reproducibility, the direction of the traveling field was inversed. The direction of the liquid flow (Fig. 8 A > B > C) was inversed as expected (Fig. 8 D > E > F). The speed of the pumped liquid was frequency dependent, as shown in Fig. 9. The peak speed $v = 140$ μm/s was found at $f = 500$ kHz, which is very close to the frequency previously predicted by impedance spectroscopy.

V. CONCLUSIONS

A micropump principle based on the application of dielectrophoretic forces on the liquid has been presented. The necessary out-of-phase polarization of the liquid volume required to apply a force on it as it is exposed to a traveling field is obtained by structural dispersion due to the *RC* behavior between the insulating electrode coating and the conductive liquid. This makes the mechanism independent of bulk-inherent dispersion and interface effects used by other micropump devices. The analysis of the device by a basic *RC* model allows to determine the operating conditions and simultaneously shows that optimized pumping force corresponds to the crossover of the complex cell impedance. This coincidence is exploited in the experimental setup by using impedance spectroscopy to monitor and adjust the operating conditions. Since the operating principle is based on structural dispersion, the optimum frequency for a given fluid conductivity can be made considerably lower than the dielectric relaxation frequency of the medium or vice versa, at a given frequency a more conductive liquid can be pumped by appropriately choosing the dimensions of the device. The analytic section describes the method comprehensively. Due to the geometrical simplifications, a precise numerical modelization by a finite element method will however be a remaining task if the method is to be developed further for future applications.

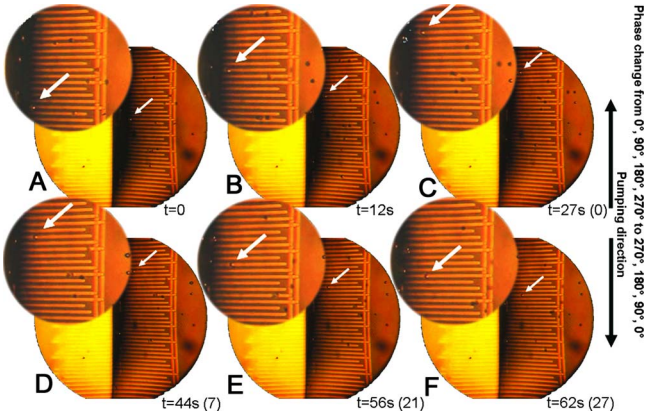

FIG. 8. (Color online) Sequences from the liquid pumping movies. Drive voltage 8 V, electrode width 6 μm, and electrode spacing 6 μm.

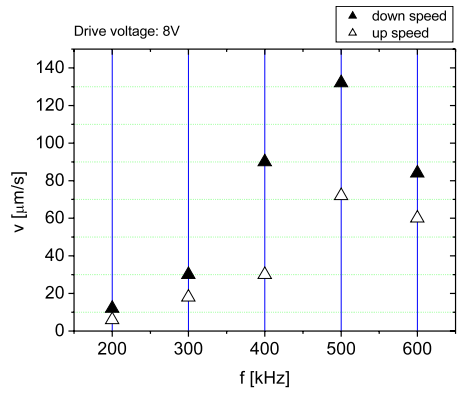

FIG. 9. (Color online) Liquid pumping speed v (μm/s) vs frequency f (kHz).

ACKNOWLEDGMENTS

M.M. acknowledges financial support from the ANR under Grant No. JC05_46152, NANOFILOUS under Contract No. ENK5-CT-2002-8066, and CEPHOMA. This work has been also supported in part by a PHC Project No. 17806NL.

[1] G. M. Whitesides, Nature (London) **442**, 368 (2006).
[2] D. Janasek, J. Franzke, and A. Manz, Nature (London) **442**, 374 (2006).
[3] R. Daw and J. Finkelstein, Nature (London) **442**, 367 (2006).
[4] A. J. deMello, Nature (London) **442**, 394 (2006).
[5] C.-M. Cheng and C.-H. Liu, J. Microelectromech. Syst. **16**, 1095 (2007).
[6] N. Islam, A. Zaman, and J. Wu, Proceedings of the IEEE Southeastcon, 2008 (unpublished), p. 27.
[7] T. S. J. Lammerink, M. Elwenspoek, and J. H. J. Fluitman, Proceedings of the IEEE Micro Electro Mechanical Systems: An Investigation of Micro Structures, Sensors, Actuators, Machines and Systems, 1993 (unpublished), p. 254.
[8] N. G. Green and H. Morgan, J. Phys. D **30**, L41 (1997).
[9] H. Morgan, N. G. Green, M. P. Hughes, W. Monaghan, and T. C. Tan, J. Micromech. Microeng. **7**, 65 (1997).
[10] R. Hagedorn, G. Fuhr, T. Müler, and J. Gimsa, Electrophoresis **13**, 49 (1992).
[11] G. Fuhr, R. Hagedorn, T. Müler, W. Benecke, B. Wagner, and J. Gimsa,

Stud. Biophys. **140**, 79 (1991).
[12]J. R. Melcher, Phys. Fluids **9**, 1548 (1966).
[13]J. R. Melcher and M. S. Firebaugh, Phys. Fluids **10**, 1178 (1967).
[14]A. Ramos, H. Morgan, B. G. Green, A. Gonzáles, and A. Castellanos, J. Appl. Phys. **97**, 084906 (2005).
[15]J. Urbanski, T. Thorsten, J. Levitan, and M. Z. Bazant, Appl. Phys. Lett. **89**, 143508 (2006).
[16]M. P. Hughes, Nanotechnology **11**, 124 (2000).
[17]P. Van Gerwen, W. Laureyn, W. Laureys, G. Huyberechts, M. O. De Beck, K. Baert, J. Suls, W. Sansen, P. Jakobs, L. Hermans, and R. Mertens, Sens. Actuators B **49**, 73 (1998).
[18]K. Asami, J. Phys. D **39**, 492 (2006).
[19]J. Gimsa and D. Wachner, Biophys. J. **75**, 1107 (1998).
[20]N. G. Green, A. Ramos, and H. Morgan, J. Electrost. **56**, 235 (2002).
[21]T. B. Jones, IEEE Eng. Med. Biol. Mag. **22**, 33 (2003).
[22]C. H. Kua, Y. C. Lam, C. Yang, K. Youcef-Toumi, and I. Rodriguez, J. Electrost. **66**, 514 (2008).
[23]K. Sekine, Bioelectrochemistry **52**, 1 (2000).
[24]L. Yang, Talanta **74**, 1621 (2008).
[25]P. Patel and G. H. Markx, Enzyme Microb. Technol. **43**, 463 (2008).
[26]M. Varshneya and Y. Li, Biosens. Bioelectron. **24**, 2951 (2009).
[27]L. Benguigui and I. J. Lin, Am. J. Phys. **54**, 447 (1986).
[28]L. Benguigui and I. J. Lin, J. Appl. Phys. **53**, 1141 (1982).
[29]H. A. Pohl, *Dielectrophoresis* (Cambridge University Press, Cambridge, 1978).